Experimental and theoretical electronic distributions in Al-Cu-based alloys

Guy Trambly de Laissardière
Laboratoire d'Etudes des Propriétés Electroniques des Solides, Centre National de la Recherche Scientifique, and Groupement de Recherche—Concertation pour l'Investigation des Quasicristaux, 25 Avenue des Martyrs, Boîte Postale 166X, 38042 Grenoble, France

Zoltán Dankházi
Laboratoire de Chimie Physique Matière et Rayonnement, URA CNRS 176, and Groupement de Recherche—Concertation pour l'Investigation des Quasicristaux, 11 rue Pierre et Marie Curie, 75231 Paris Cedex 05, France and Institute for Solid State Physics, Muzéum krt 6-8, 1088 Budapest, Hungary

Esther Belin
Laboratoire de Chimie Physique Matière et Rayonnement, URA CNRS 176, and Groupement de Recherche—Concertation pour l'Investigation des Quasicristaux, 11 rue Pierre et Marie Curie, 75231 Paris Cedex 05, France

Anne Sadoc
Laboratoire pour l'Utilisation du Rayonnement Electromagnétique, Centre National de la Recherche Scientifique, Commissariat à l'Energie Atomique, and Groupement de Recherche—Concertation pour l'Investigation des Quasicristaux, Université Paris-Sud, 91405 Orsay Cedex, France and Laboratoire de Physique des Matériaux et des Surfaces, Université de Cergy-Pontoise, 95806 Cergy-Pontoise Cedex, France

Nguyen Manh Duc and Didier Mayou
Laboratoire d'Etudes des Propriétés Electroniques des Solides, Centre National de la Recherche Scientifique, and Groupement de Recherche—Concertation pour l'Investigation des Quasicristaux, 25 Avenue des Martyrs, Boîte Postale 166X, 38042 Grenoble, France

Michael A. Keegan
Computational Sciences and Informatics Institute, George Mason University, Fairfax, Virginia 22030

Dimitrios A. Papaconstantopoulos
Complex Systems Theory Branch, Naval Research Laboratory, Washington, D.C. 20375-5345
(Received 13 June 1994; revised manuscript received 26 October 1994)

We report on experimental and calculated occupied and unoccupied electronic distributions of crystalline Al_2Cu and various Al-Cu-Fe alloys. The experiments have been carried out by means of soft-x-ray-spectroscopy and photoelectron-spectroscopy techniques. The densities of states have been calculated using either the linear-muffin-tin-orbital atomic-sphere-approximation or the augmented-plane-wave methods. The comparison between experiment and calculations is discussed. We pay special attention to the effect of Fe in the various alloys and emphasize the role of Al atom neighbors. We propose that changes in Al site occupancy that induce changes in Al p-d hybridization near the Fermi level could be responsible for the modifications of the densities of states observed in quasicrystalline Al-Cu-Fe phases with respect to the crystalline Al-Cu_2Fe alloy.

I. INTRODUCTION

Numerous investigations have been carried out since the discovery of the fivefold rotational symmetry in rapidly quenched alloys, the so-called quasicrystals. Such investigations aim to ascertain the atomic and electronic structure of quasicrystals. Also, for comparison, emphasis is given to the study of crystalline alloys of related nominal composition

Many systems involving the fivefold rotational symmetry are alloys of elements that have small differences in atomic radii and electronegativities. As a first approximation, these systems could be considered as Hume-Rothery-like alloys.[1] This has been confirmed by x-ray diffraction patterns, which show that Bragg planes of spots with high intensities are near the Fermi surface.[2] The diffraction by such Bragg planes is well known to induce a pseudogap near the Fermi level (E_F). Actually, a pseudogap at E_F has been seen in quasicrystals from experimental investigation of occupied and unoccupied states distributions using soft x-ray and photoelectron spectroscopies (respectively, SXS and XPS) as reported

elsewhere.[3–6] The results showed that in the vicinity of E_F there are low densities of states (DOS) and that there is a noticeable depletion of both occupied and unoccupied Al states.[3–8] Such a pseudogap near the E_F may be expected in crystalline phases of composition close to that of the quasicrystals. Indeed, a not very pronounced pseudogap has been found by experimental and theoretical means for crystalline Al_6Mn that is close to the $Al_{86}Mn_{14}$ quasicrystal.[9] The important role played by hybridization between *sp* and *d* states has also been pointed out: theoretical studies have emphasized that the *sp-d* hybridization tends to increase the pseudogap and leads to a splitting of the *d* bands.[10–13]

In this paper we present a comparison between the experimental electronic distributions of crystalline Al_2Cu, Al_7Cu_2Fe, $Al_{55}Cu_{33}Fe_{12}$, and $Al_{46}Cu_{36}Fe_{18}$ and calculated partial occupied and unoccupied DOS's for Al_2Cu, Al_7Cu_2Fe, $Al_{68.75}Cu_{18.75}Fe_{12.5}$, and $Al_{50}Cu_{37.5}Fe_{12.5}$. The experiments have been carried out using the SXS and XPS techniques. The electronic structures have been calculated in the framework of *ab initio* models using either the linearized muffin-tin-orbital (LMTO) method in the atomic-sphere-approximation (ASA), or the augmented-plane-wave (APW) method both within the local-density approximation (LDA).

The paper is organized as follows: First, we summarize the principles of the experimental techniques and give the results that we have obtained. Second, we summarize the methodology of the calculations and detail the results for the total and partial DOS's of the various alloys. Finally, we compare and discuss the experimental and theoretical data. In this section, we also present a brief comparison between crystalline Al_7Cu_2Fe and a quasicrystalline alloy of composition $Al_{63}Cu_{35}Fe_{12}$.

II. EXPERIMENTS

A. Experimental procedure

The investigation of the electronic states distributions was carried out by means of soft-x-ray-emission-spectroscopy (SXES) and soft-x-ray-absorption-spectroscopy (SXAS) techniques. Indeed, SXES and SXAS are known to provide separately information on occupied and unoccupied electronic distributions because the x-ray transitions involve, respectively, an inner level of the sample and either outest filled or first empty band states (occupied and unoccupied bands denoted, respectively, OB and UB). These transitions are partial because they are governed by dipole selection rules and they are also local since the inner level belongs to a specific atom in the sample. Since the measured spectral intensities are proportional to the result of the convolution of the partial OB or UB DOS's and the energy distribution of the inner level involved in the x-ray transition, the shapes of the experimental x-ray spectra are directly related to those of the corresponding DOS's. However, the x-ray transitions are also dependent on x-ray transition probabilities. We note that in the analyzed spectral ranges, usually these transition probabilities are taken to be constant since they vary slowly as a function of energy. It is to be mentioned that in the case of transitions involving the *p* inner level, *d* and *s* states are concerned but transitions to or from *d*-like states are favored with respect to transitions to or from *s*-like states.

In SXES experiments, the electronic distribution curves deduced from the spectra are normalized to their maximum intensity. In SXAS measurements, generally the curves are normalized between ranges before and after the absorption edges where the variation of intensity is negligible. Thus, no absolute DOS values can be derived from the experiments; however, it is possible to compare curves of a given spectral character in various samples.

Using XPS we measured the binding energies of the inner levels involved in the x-ray processes with respect to the Fermi level by calibrating the energy scale for C 1*s* at 285.0 eV. We could not measure directly the binding energy of the Al 1*s* level. To obtain this latter value, we measured the binding energy of the Al $2p_{3/2}$ level and also the energy of the Al *Ka* line, i.e., the x-ray transition $2p_{3/2} \rightarrow 1s$. Finally, it was possible to locate the Fermi level on the energy scale corresponding to each x-ray transition. As a consequence, the various partial electronic distributions could be adjusted in a unique binding-energy scale with the Fermi level as the origin. This kind of adjustment allows us to describe separately OB and UB and makes it possible to gain insight into the various electronic interactions in the solid.

We have studied several alloys: crystalline Al_2Cu, $Al_{55}Cu_{33}Fe_{12}$, $Al_{46}Cu_{36}Fe_{18}$, and Al_7Cu_2Fe (denoted as *w* phase) as well as quasicrystalline icosahedral $Al_{63}Cu_{25}Fe_{12}$. We indicate in Table I the different SXS transitions, which we analyzed in order to investigate OB

TABLE I. Analyzed x-ray transitions, energy range, and energy resolutions.

SXS line	Transition	Valence states	Conduction states	Energy range (eV)	Energy resolution (eV)
Al $K\beta$	$1s \leftarrow$OB	3*p*		1545–65	0.2
Al $L_{2,3}$	$2p \leftarrow$OB	3*s*,*d*		60–75	0.3
Fe $L\alpha$	$2p_{3/2} \leftarrow$OB	3*d*-4*s*		700–10	0.3
Cu $L\alpha$	$2p_{3/2} \leftarrow$OB	3*d*-4*s*		920–35	0.3
Al *K*	$1s \rightarrow$UB		*p*	1555–65	0.5
Fe *K*	$1s \rightarrow$UB		*p*	7100–15	0.5
Cu *K*	$1s \rightarrow$UB		*p*	8970–85	0.5
Fe *L*	$2p_{3/2} \rightarrow$UB		*d*-*s*	710–50	0.3
Cu *L*	$2p_{3/2} \rightarrow$UB		*d*-*s*	930–50	0.3

and UB states; the corresponding spectral energy resolutions are also given in this Table I.

To investigate OB states, the measurements were performed in vacuum spectrometers fitted with bent crystals or a grating and electronic detection.[3,4] Due to the so-called "secondary excitation technique" or "fluorescence technique" used for obtaining the valence Fe and Cu La bands, no oxide contribution is expected for the corresponding Fe and Cu spectra. However, there is oxide contribution in the occupied Al subbands, obtained by irradiating the samples with incoming electrons. Whereas the Al $3p$ emission bands can be corrected exactly for this extra emission due to oxide, this could not be achieved for the Al $3s,d$ bands. Thus, an oxide contribution to the spectra was estimated and removed from the raw data; consequently, the shape of these curves is not exactly in the energy range corresponding to the same emission in Al_2O_3, i.e., within E_F+4 to E_F+6 eV.

The UB states were analyzed at the synchrotron facility of LURE (Orsay, France). Cu and Fe p states were obtained at (DCI) in the photoabsorption transmission mode using a Si 331 channel-cut monochromator. The Al p, Fe d, and Cu d states were probed at Super-(ACO).[6]

The XPS measurements were performed with a Kratos spectrometer fitted with a Mg anode used in such conditions that the full width at half maximum intenstiy of the Ag $3d_{5/2}$ peak is 1 eV. The experimental estimated errors are ± 0.1 eV for the Al $2p_{3/2}$ level and ± 0.3 to ± 0.5 eV for the $2p_{3/2}$ level of the other elements.

B. Results

The shapes of the Fe $3d$ and Cu $3d$ distributions in the alloys are not significantly affected with respect to the pure metal. However, in the alloys, the full width at half maximum (FWHM) of the curves is reduced by 0.8 ± 0.1 eV for Fe and 0.5 ± 0.1 eV for Cu. All the same, the maxima of the distributions are shifted towards E_F in the case of Fe by 0.6 ± 0.1 eV and towards the center of the OB for Cu by 1.0 ± 0.1 eV. On the contrary, the shapes of the Al distributions are strongly modified in the alloys with respect to the pure metal. The distributions in pure Al are paraboliclike with a narrow peak near the Fermi level for the partial s,d distribution; this narrow peak is due to both the presence of d-like states and to many-body effects.[14,15] On the contrary, in the alloys, the Al subbands are noticeably structured.

Figure 1 displays the OB curves for Al_2Cu. The Cu $3d$ OB states are located in the middle of the band, at about E_F+4 eV. Their interaction with the Al states makes the Al s-d and p subbands split into two parts located on each side of the Cu $3d$ distribution in agreement with previous results;[16,17] the corresponding maxima are at $E_F+1.0$ and at $E_F+4.95$ eV for Al $3p$ states distributions and $E_F+0.9$ and at $E_F+5.5$ eV for Al $3s,d$ states distributions. The figure shows that the Al partial electronic distributions overlap on the whole valence band; consequently, Al subbands are totally hybridized.

For $Al_{46}Cu_{36}Fe_{18}$, $Al_{55}Cu_{33}Fe_{12}$, and Al_7Cu_2Fe, the Al subbands also are split into two parts and the Cu $3d$ states lie in between them, in the middle of the OB, as shown in Figs. 2 and 3. For these alloys, the Fe $3d$ OB states are present in the vicinity of E_F, the maximum of the distribution being at about $E_F+1.3$ eV. The DOS's at E_F are slightly decreased with comparison to pure Al: the Al $3p$ DOS at E_F is 50% for pure Al, it is only 40% for Al_2Cu, and about 32% for $Al_{46}Cu_{36}Fe_{18}$, $Al_{55}Cu_{33}Fe_{12}$, and Al_7Cu_2Fe. This decrease of intensity at the Fermi level reveals the formation of a small pseudogap at E_F in these alloys and, thus, provides evidence that they are Hume-Rothery-like alloys.

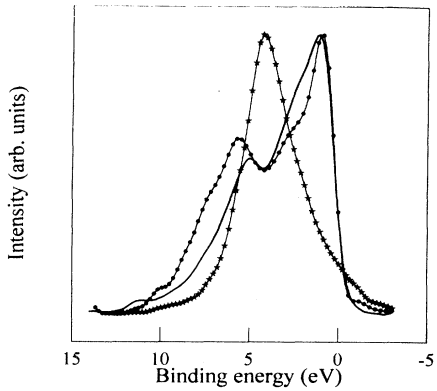

FIG. 1. Valence band of Al_2Cu: full line is Al $3p$ distribution, line with full circles is Al $3s,d$ distribution, line with stars is Cu $3d$ distribution.

Figure 4 displays Al_7Cu_2Fe UB curves. The first conduction states are Fe s,d in interaction with Al p states, beyond about 2 eV from the edges, all the Fe d-s and p, Al p together with Cu d-s and p curves overlap revealing that the corresponding states interact over the whole extent of the UB, which we have investigated. However, while the Al, Fe, and Cu p states are completely mixed, the interaction is not so strong in ranges where there are minima in the curves, i.e., at about E_F-4 eV and E_F-7 eV for Fe d-s states, and E_F-7 eV for both Fe d-s and Cu d-s states.[4,6]

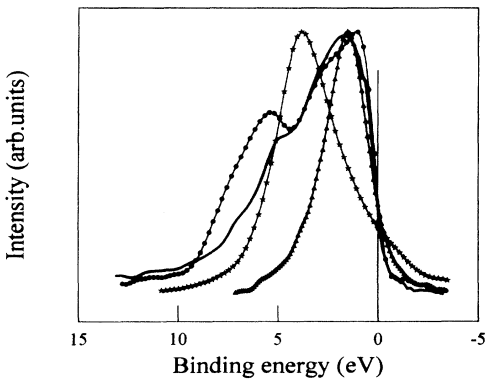

FIG. 2. Valence band of Al_7Cu_2Fe: full line is Al $3p$ distribution, line with full circles is Al $3s,d$ distribution, line with triangles is Fe $3d$ distribution, line with stars is Cu $3d$ distribution.

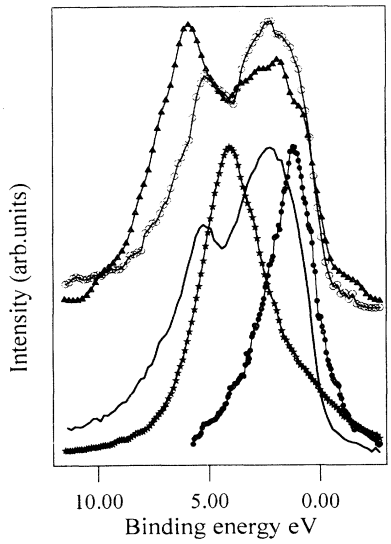

FIG. 3. Lower curves are the occupied band of $Al_{55}Cu_{33}Fe_{12}$, full line is Al $3p$ distribution, line with full circles is Al $3s,d$ distribution, line with stars is Cu $3d$ distribution, * upper curves are the occupied band of $Al_{46}Cu_{36}Fe_{18}$, line with open circles is Al $3p$ distribution, line with triangles is Al $3s,d$ distribution.

III. CALCULATIONS

A. Techniques

We have performed a self-consistent relativistic LMTO calculation in the ASA (Refs. 18 and 19) for Al_2Cu and Al_7Cu_2Fe, respectively, in the body-centered-tetragonal structure[20] and the primitive tetragonal structure.[21] In the framework of the atomic sphere approximation, the spheres radii are chosen so that the total volume of the spheres equals that of the unit cell.

For Al_2Cu the lattice parameters are $a=6.04$ Å and $c=4.86$ Å with the space group $D_{18/4h}$-$p4/mcm$ ($C16$). In this AB_2 structure, there are six atoms per unit cell, as shown in Fig. 5(a), but a better visual representation comes from the fact that the A atoms form parallel linear chains throughout the system, each A chain being strung out with squares of B atoms as shown in Fig. 5(b). Squares are positioned halfway between the A atoms and are rotated so that there is an angular alteration between successive squares. The positions of the atoms in the unit cell are shown in Table II.[20] In the resulting arrangement, each aluminum has four copper neighbors at a distance of 2.59 Å and an aluminum atom at 2.70 Å. On the other hand, each copper atom has two copper neighbors with Cu-Cu=2.43 Å and eight aluminum atoms at 2.59 Å. In the LMTO calculation, the sphere radii are $R_{Al}=1.58$ Å and $R_{Cu}=1.42$ Å. Thus, the ratio is $R_{Cu}/R_{Al}=0.9$. We include Al ($3s,3p,3d$), Cu ($4s,4p,3d$) levels as occupied states. The self-consistent electronic structure was derived from a grid of 180 irreducible **k** points (i.e., 1000 **k** points in the Brillouin zone) and the eigenvalues were used to calculate the DOS with the tetrahedron method.[22]

For Al_7Cu_2Fe the lattice parameters are $a=6.33$ Å and $c=14.81$ Å and the space group is $P4/mnc$.[23,24] There are 40 atoms in the unit cell (Fig. 6), their positions correspond to five different Wyckoff positions defined as shown in Table III. Inspection of the nearest neighbors allows us to note that (Table IV) (i) the Fe(e) atoms have the coordination 9 and are surrounded only by Al atoms [four Al (3), four Al (2) and one Al (1)]; (ii) the Cu (h) atoms have the coordination 11, they are surrounded by three Cu, six Al (3) and two Al (1) atoms and there are no Al (2) atoms in the nearest-neighbors shell; (iii) the mean contact distances for Fe-Al, Cu-Al, and Al-Al are 2.477, 2.594, and 2.865 Å, respectively. This may account for

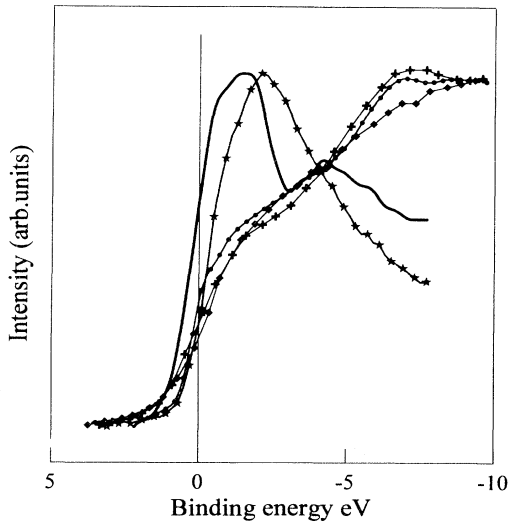

FIG. 4. Conduction band of Al_7Cu_2Fe: full line is Fe d,s distribution, line with stars is Cu d,s distribution, line with full circles is Al p distribution, line with rectangles is Fe p distribution, line with crosses is Cu p distribution.

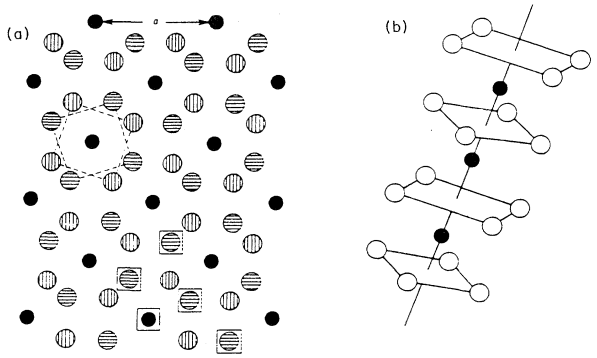

FIG. 5. (a) AB_2 structure: the primitive cell contains six atoms (squares): two consecutive A atoms and four B atoms at an intermediate level. Projection perpendicular to the c axis: A atoms (full circles) at $c=\ldots,-c/4,c/4,3c/4$, B atoms (vertical hatched circles) at $c=\ldots,-c,0,c,\ldots$, B atoms (horizontal hatched axis) at $c=\ldots,-c/2,c/2,3c/2,\ldots$ ideal c value: $a\sqrt{2/3}$. (b) Chain of A atoms strung with squares of B atoms. Alternate squares are rotted as shown in (a).

TABLE II. Coordinates of the atoms in the unit cell of Al_2Cu ($u=0.160$).

Atom	Site coordinaates		
Cu	0	0	$-\frac{1}{4}$
Al	u	$u-\frac{1}{2}$	0
Al	$-u$	$\frac{1}{2}-u$	0
Al	$\frac{1}{2}-u$	u	0
Al	$u-\frac{1}{2}$	$-u$	0

TABLE III. Positions and coordinates of the atoms in the unit cell of Al_7Cu_2Fe.

Atom	Wyckoff notation	x	y	z
Al [1]	4 (e)	0.0	0.0	0.134
Al [2]	8 (g)	0.165	0.665	0.250
Al [3]	16 (i)	0.198	0.420	0.100
Cu	8 (h)	0.278	0.088	0.0
Fe	4 (e)	0.0	0.0	0.2992

the fact that, in this structure, the interaction between Fe-Al and Cu-Al is stronger than that between Al-Al atoms.

The sphere radii are $R_{Al}=1.55$ Å, $R_{Cu}=1.48$ Å, and $R_{Fe}=1.39$ Å. Thus, the radii ratios are $R_{Cu}/R_{Al}=0.95$ and $R_{Fe}/R_{Al}=0.90$. There is an overlap of 30% between neighboring spheres; this is reasonable in LMTO calculations.[18,25] Note that this choice corresponds to the minimal excess numbers of electrons in each atomic sphere and, thus, cannot be considered as a genuine "charge transfer."[26]

A scalar relativistic LMTO-ASA code[27] with the combined corrections, which account for the finite number of terms in the angular-momentum expansions, has been used. It includes terms with $l \leq 2$, which means that the Al ($3s,3p,3d$), Cu ($4s,4p,3d$), and Fe ($4s,4p,3d$) levels are used as OB states. Exchange and correlation were treated within the local-density approximation using the formalism of von Barth and Hedin.[28]

The self-consistent electronic structure was derived from a grid of 60 irreducible **k** points (i.e., 384 **k** points in the Brillouin zone) and the eigenvalues were used to calculate the DOS's with the tetrahedron method. The iterating to self-consistency process was stopped when the total energies of all the atoms changed by less than 10^{-2} mRy. We have carried out the *ab initio* calculation in a spin-polarized mode and the results shows that the magnetic effects on Fe are negligible in Al_7Cu_2Fe; so, in the following, we will refer to LMTO calculation in the paramagnetic case.

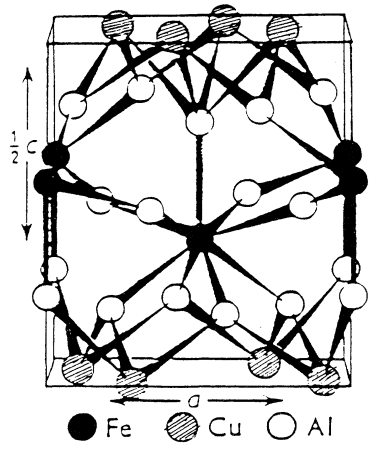

FIG. 6. One-half of the unit cell of Al_7Cu_2Fe.

The APW method[29] was used to calculate energy bands and density of states for model alloys with nominal composition near the composition of alloys measured as described above. These APW calculations were performed self-consistently with scalar relativistic terms within the muffin-tin approximation. The exchange and correlation of electrons are treated within the local-density approximation according to the parametrization of Hedin and Lundqvist.[30] In order to model ternary alloys, we have used two different supercells: (1) an 8-atom supercell with bcc symmetry and (2) a 16-atom supercell with simple cubic symmetry. The 8-atom supercell permits calculation for a model alloy with nominal composition Al_4Cu_3Fe, i.e., $Al_{50}Cu_{37.5}Fe_{12.5}$. The 16-atom cell has slightly more flexibility to come close to the experimental compositions presented in this paper. We have performed calculations for the composition $Al_{11}Cu_3Fe_2$, i.e., $Al_{68.75}Cu_{18.75}Fe_{12.5}$. For all three elements, equal sphere radii were used, scaled according to the lattice constant, at the lattice site to form nonoverlapping spheres. The lattice parameters determined from total-energy calculations are 5.78 and 5.91 Å for the 8-atom and 16-atom cells, respectively. Lattice sites and atom type occupying the sites for these model alloys are tabulated in Table V.

TABLE IV. Distances and number of first neighbors in Al_7Cu_2Fe. (1), (2), and (3) denote the different Al sites in this structure.

Atom	Neighbor	Number of atoms	Distance (Å)
Cu	Cu	2	2.613
	Cu	1	3.026
	Al [3]	2	2.511
	Al [3]	2	2.522
	Al [3]	2	2.625
	Al [1]	2	2.717
Fe	Al [3]	4	2.483
	Al [2]	4	2.477
	Al [1]	1	2.456
Al [1]	Al [3]	4	2.985
	Al [2]	4	2.928
Al [2]	Al [3]	2	2.726
	Al [3]	2	2.888
	Al [3]	2	3.259
	Al [2]	1	2.957
	Al [2]	4	3.346
Al [3]	Al [3]	1	2.706
	Al [3]	2	2.799
	Al [3]	2	2.974

TABLE V. Coordinates of lattice for the 8-atom and 16-atom supercells with body-centered-cubic and simple cubic symmetry, respectively. The lattice sites for the 8-atom cell are in parentheses. (Note that for the 8-atom cell, some of the sites of the 16-atom cell are equivalent under a translation by a lattice vector. These sites do not list the atom type in parentheses.) Atom types are given for the compositions discussed in the text.

Site	Coordinates	Atom type 16-atom [8-atom] supercell
Cube corner	[0,0,0]	Fe [Fe]
Body center	[0.5,0.5,0]	Fe
	[0.5,0.5,0]	Al [Cu]
Face center	[0.5,0,0.5]	Al [Cu]
	[0,0.5,0.5]	Al [Cu]
	[0.25,0.25,0.25]	Al [Al]
	[0.25,0.25,0.75]	Al
	[0.25,0.75,0.25]	Al
Tetrahedral	[0.75,0.25,0.25]	Al
	[0.75,0.75,0.25]	Al [Al]
	[0.25,0.75,0.75]	Al [Al]
	[0.75,0.25,0.75]	Al [Al]
	[0.75,0.75,0.75]	Al
Midpoint	[0.5,0,0]	Cu
of cube	[0,0.5,0]	Cu
edge	[0.0,0.5]	Cu

Specifically, Table V gives the lattice sites for the 16-atom cell explicitly, then for the 8-atom cell in parenthesis. Since the 8-atom cell is of bcc symmetry some of the sites of the 16 atom are equivalent under a propagation by a lattice vector, only the inequivalent sites of the 8-atom cell are listed in the Table.

The computational complexity of these APW calculations is proportional to the number of atoms in the unit cell. To perform these calculations more efficiently we have block diagonalized the secular equation using the group symmetry of the cubic supercells. Iteration to self-consistency was performed on a mesh of 14 **k** points in the 1/48th of the Brillouin zone for the 8-atom supercell and 10 **k** points in the 1/48th of the Brillouin zone for the 16-atom supercell. These **k**-point meshes are equivalent to 128 and 64 **k** points in the full Brillouin zone, respectively. The number of **k** points required to achieve accuracy on the order of 0.1 mRy is small for supercell calculations, primarily due to folding of states back into the zone. We have also used Broyden mixing to reduce the number of cycles required to reach self-consistency, specifically, we have used the second formulation of Broyden's method.[31]

The energy bands were interpolated to 969 points within the irreducible wedge of the Brillouin zone[32] and input to a calculation of the DOS according to the tetrahedron method.[21] DOS was calculated at the theoretical equilibrium lattice constant determined by analyzing the total energy as a function of the lattice constant for each compound. In order to make a more meaningful comparison with the SXS experiments (see the paragraph discussion), we have included plots of the DOS that have been broadened to account for the inner level involved in the x-ray transitions and summed according to the spectral measurement. For the K spectra, we have simply broadened the p DOS. For the L spectra, we have added the s DOS with two-fifths of the d DOS and applied the broadening. The theoretical basis for this procedure is found in the work of Goodings and Harris.[33] And as pointed out earlier, transition probabilities are constant or nearly constant and not required to be included for meaningful comparison.

B. Results

1. Al_2Cu

Figure 7, top panel, displays the total Al_2Cu DOS obtained with the LMTO calculation. The Fermi level lies close to a minimum of the DOS. The OB states show an intense set of peaks of about 21 and 14 states/eV at about 4 eV from E_F; both OB and UB states are low and faintly structured around E_F.

The partial Cu d OB DOS's curve given Fig. 7, second panel from the top, consists principally of a set of intense peaks centered at about 4 eV below E_F. These Cu OB d states, of about 18.4 states/eV, are the dominant states of the total DOS's and extend over about 3 eV. We pointed out that Cu p and s states do not significantly contribute to the OB since their maxima are about 50 times less intense than the Cu d states. The Cu d UB states are of very low intensity and seem to be almost constant (less than 0.75 states/eV). The same is true for Cu s and p UB states, which are not shown here.

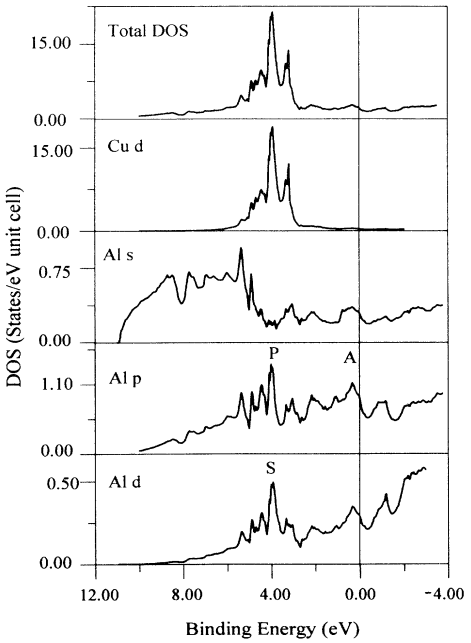

FIG. 7. Calculated total and partial densities of states of Al_2Cu. From top to bottom: total DOS and Cu d, Al s, Al p, and Al d distributions.

We plot also in Fig. 7, in the three lower panels, respectively, the partial Al d, s, and p DOS's. In the OB, the maximum densities of states are of about 0.75 states/eV for Al d distribution, 0.89 states/eV for Al s, and 1.47 states/eV for Al p states distributions. Al s states are present mainly in the range from 4 to 11 eV below E_F. They overlap p and d states in the energy range around 4 eV below E_F so they are slightly s-p-d hybridized. In the high binding region of the OB, beyond 8 eV below E_F, the states are almost pure Al s. In all the Al partial DOS's curves, there is a peak, denoted A in the Al p curve, that shows the states are also s-p-d like in this energy range near the Fermi level. At the energy of the intense peak of the partial Cu d DOS curve, a set of peaks is also present on the Al p and Al d DOS curves, they are labeled as P and S, respectively. In the UB energy range, the curves corresponding to Al s, p, and d DOS overlap and have little structure; thus, the conduction Al states are totally s-p-d hybridized. Similarly, the Cu s, p, and d UB states (the s and p are not shown here) overlap with the Al states. As a consequence, Al states interact with Cu states over the UB energy range.

2. Al_7Cu_2Fe

We present in Fig. 8, top panel, the total DOS curve for Al_7Cu_2Fe. Both the occupied and empty DOS's exhibit a somewhat spiky shape and the Fermi energy lies in a minimum of the total DOS. Intense OB states of about 88 states/eV are present around 4 eV below E_F; other intense peaks of 37 states/eV are located at $+2$ eV then the intensity decreases near E_F and it is about 11 states/eV at E_F.

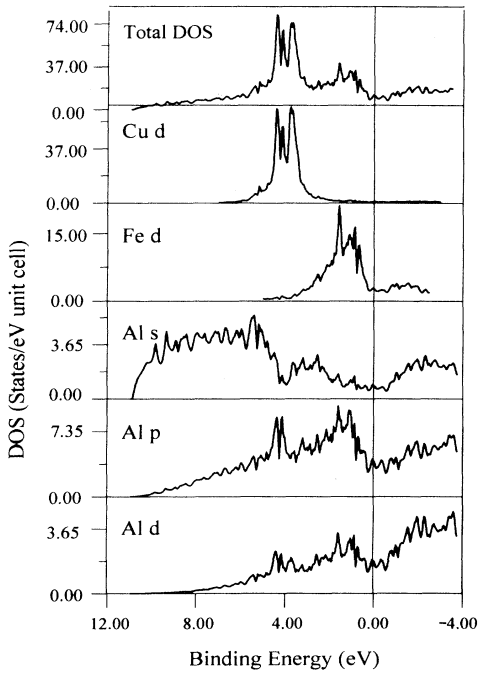

FIG. 8. Calculated total and partial densities of states of Al_7Cu_2Fe. From top to bottom: total DOS and Cu d, Fe d, Al s, Al p, and Al d distributions.

The partial DOS's are displayed in the same figure. The Cu d OB DOS's curve exhibits an intense peak (66.2 states/eV) of about 2 eV wide, located approximately 4 eV below E_F in the OB region. These Cu OB d states are the dominant states of the total DOS's. Similar to Al_2Cu, the Cu p and s states do not significantly contribute to the OB since their maxima are, respectively, 2.2 and 0.9 states/eV so they are not plotted here.

The Fe d OB DOS's curve consists of a set of narrow intense peaks (22 states/eV) of about 2.5 eV wide, located approximately at 1.5 eV below E_F. The s states spread over 10 eV, their mean intensity value is 0.3 states/eV. The p states, increase monotonically from 10 eV below E_F to E_F, the maxima, at 1.5 eV is 1.1 states/eV. These s and p states are not shown on the figure since they do not play a significant role in the OB.

The partial Al s, p, and d DOS curves correspond to the sum of the contributions for all the different Al sites. All these curves are quite spiky. In OB, Al s states concentrate mainly in the range between 4 to 11 eV below E_F, the mean intensity is 4.4 states/eV. The p and d states increase monotonically from the high binding states to E_F; their respective maxima are at $+1.5$ eV and the corresponding intensities are about 11 and 2.9 states/eV, respectively. In the range between E_F and 4 eV below E_F, all the Al states overlap so they are s-p-d hybridized whereas the states in the high-binding-energy region of the OB are almost pure Al s. The Al DOS's are superposed to the Cu d DOS at about 4 eV below E_F and to the Fe d DOS at about 1.5 eV below E_F. So, there is a strong interaction between the Al s and Cu d states whose result is to divide the Al s subband into two parts separated by a noticeable valley at 4 eV below E_F. There is also a strong interaction between Fe d and Al p and d states near E_F. Both Al p and d DOS's exhibit a rather prominent peak at the energy position of the maximum of the Cu d DOS. We will discuss this point later.

In the UB energy range, the curves corresponding to Al p, d, and s DOS's overlap. So, the conduction Al states are s-p-d hybridized beyond 4 eV above E_F, after that they are more p-d hybridized (beyond about 8 eV above E_F). Similarly, the UB part of Cu and Fe d, p, and s curves overlap the others in the range E_F-8 eV so the Al s-p-d hybridized states interact with Cu and Fe d states over this energy range.

Finally, we would like to comment on the splitting of the d band of Fe that is seen through the formation of a pseudogap around E_F. Usually, the splitting of d bands is caused by crystal field, spin-orbit coupling, or covalency splitting as explained in Ref. 34 (and references cited therein). In the case of Al_7Cu_2Fe, like for other systems where the diffraction of free electrons by Bragg planes is strong near E_F, the origin of this splitting is due to the sp-d hybridization term of the Hamiltonian as shown in Ref. 10.

3. $Al_{50}Cu_{37.5}Fe_{12.5}$

Figure 9 shows the total DOS for $Al_{50}Cu_{37.5}Fe_{12.5}$, as calculated by the APW method. The curves correspond to the DOS for the theoretical equilibrium lattice con-

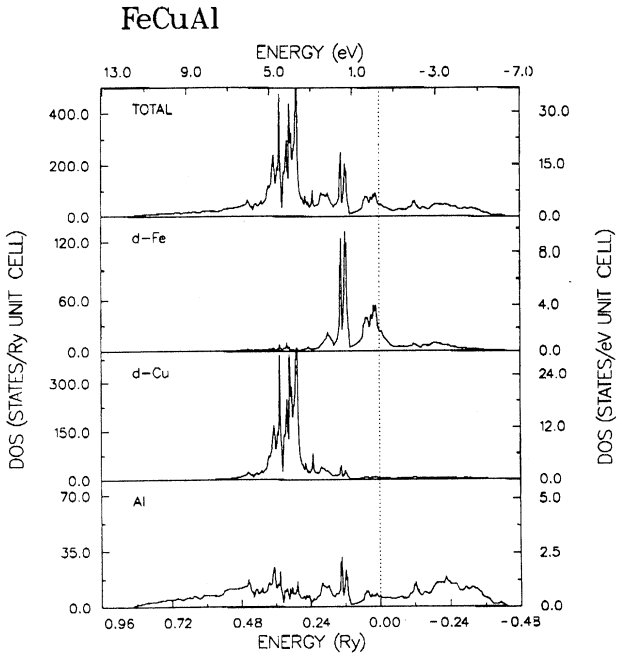

FIG. 9. Calculated total and partial densities of states of $Al_{50}Cu_{37.5}Fe_{12.5}$. From top to bottom: total DOS and Fe *d*, Cu *d*, and total Al distributions.

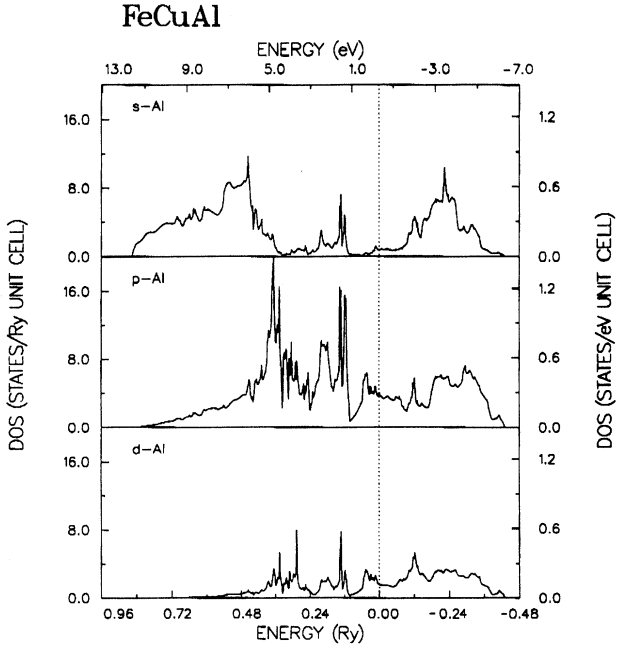

FIG. 10. Calculated partial densities of states of Al in $Al_{50}Cu_{37.5}Fe_{12.5}$. From top to bottom: Al *s*, Al *p*, and Al *d* distributions.

stant, as determined from our total-energy calculation. The Fermi level lies close to a secondary maximum in the DOS, which has a value of 6.6 states/eV. The density of states at E_F, denoted $N(E_F)$, is 3.5 states/eV. In Fig. 9 (panels 2 and 3 from the top), we have plotted only the *d*-character DOS for Fe and Cu to demonstrate that these are the dominant contributors to the total DOS. The Fe *d* DOS is split into two major features, one near E_F mentioned in the discussion of E_F and a second feature about 1.6 eV below E_F. The feature located 1.6 eV below E_F, is the second most intense in the total DOS, with a peak of 18.3 states/eV. The Cu *d* feature is the most intense in the total DOS and has a maximum of 63.75 states/eV. It is centered at about 4 eV below E_F. The Cu *d* feature extends over a 3-eV range. The UB states are mixed *s-p-d* that is, the UB states are not dominated by the *d* states of Fe and Cu. The Cu UB states are flat and their intensity is low. For Fe UB states, the intensity is low except near E_F. The bottom panel of Fig. 9 shows the total Al DOS; the intensity is very low as compared to the total DOS. The reader should note that in the APW calculations, the partial DOS are projected within the muffin-tin spheres; therefore, the sum of all partial DOS at a given energy is significantly smaller than the total DOS.

In Fig. 10, the Al partial DOS is shown: the *s* character in the top panel, the *p* character in the middle panel, and the *d* character in the bottom panel. The peaks associated with the Al *p* character are the most intense, the *s* character peaks are the next most intense, and the *d* character peaks are the least intense. In agreement with the previous DOS presented in this paper, the Al *s* states dominate in the high-binding-energy part of the OB, between 4 and 11 eV below E_F. The intensity of the *s* states becomes faint in the energy range near 4 eV, while the partial *p* and *d* distributions become intense due to interaction with the Cu 3*d* levels. Note that in each panel there are narrow peaks around 2 eV below E_F, the position of these peaks corresponds to the positions of intense peaks in the Fe *d* distribution. The Al states are *s-p-d* like in this energy range and are interacting with the Fe *d* states. This interaction, as well as the Cu 3*d*–Al 3*p-d* interaction, will be discussed in the next section.

4. $Al_{68.75}Cu_{18.75}Fe_{12.5}$

The last example is plotted in Fig. 11, which displays the total DOS and relevant partial DOS of $Al_{68.75}Cu_{18.75}Fe_{12.5}$. These curves are calculated at the theoretical equilibrium lattice constant. E_F falls near a secondary maximum as in $Al_{50}Cu_{37.5}Fe_{12.5}$. $N(E_F)$ is 5.88 states eV, a relative minimum. The Fe *d* DOS, as compared to $Al_{50}Cu_{37.5}Fe_{12.5}$, is not split widely; however, a two-peak feature remains. The intensity of the two peaks is very nearly equal, 9.62 states/eV. Furthermore, the gross property of the Fe *d* DOS can be described as less structured than in the case of $Al_{50}Cu_{37.5}Fe12.5$, apparently due to the change in atomic species at the second-nearest-neighbor sites for the Fe positioned at the cube center. For $Al_{50}Cu_{37.5}Fe_{12.5}$, the second neighbor of Fe is Cu, but it is Al in the current case. The Cu *d* DOS remains fixed in position and intensity with respect to the $Al_{50}Cu_{37.5}Fe_{12.5}$ results, the maximum has 68.2 states/eV. Above E_F, the Cu-*d* DOS is very flat and the intensity is very low. The Fe-*d* DOS above E_F shows a single feature

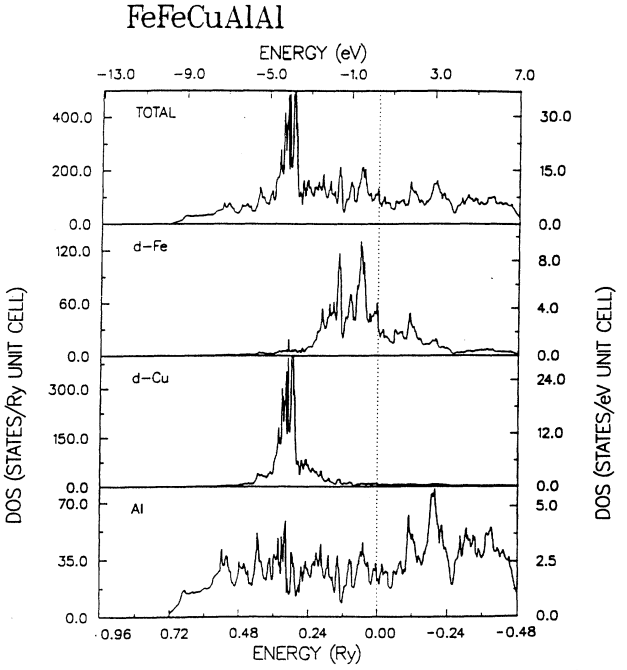

FIG. 11. Calculated partial densities of states of Al in $Al_{68.75}Cu_{18.75}Fe_{12.5}$. From top to bottom: total DOS and Fe d, Cu d, and total Al distributions.

of low intensity, 3.53 states/eV, positioned 1.5 eV from E_F.

In Fig. 12, the Al partial DOS for $Al_{68.75}Cu_{18.75}Fe_{12.5}$ are plotted in the same manner as Fig. 10. The DOS associated with Al s (top panel) is the second most intense,

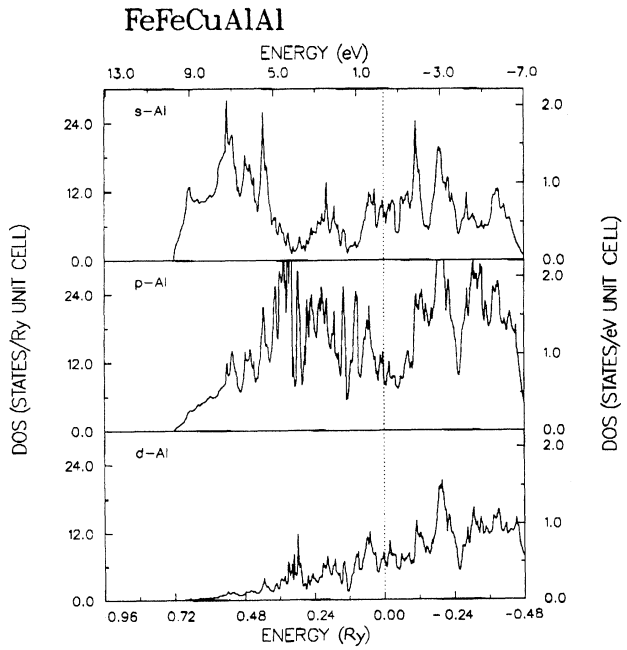

FIG. 12. Calculated partial densities of states of Al in $Al_{68.75}Cu_{18.75}Fe_{12.5}$. From top to bottom: Al s, Al p, and Al d distributions.

the DOS associated with Al p (middle panel) is the most intense, and the Al d DOS (bottom panel) is the least intense. Note that the Al d DOS shown in Fig. 12 appears to be similar to the Al d DOS calculated for Al_7Cu_2Fe (Fig. 8), monotonically increasing from the high-binding-energy region toward E_F. The only deviation from this characterization of the curve is a feature about 4 eV from E_F caused by the interaction with the Cu $3d$ states. There is a similar shape in the Al d DOS calculated for Al_7Cu_2Fe. There is little similarity between the Al partial DOS for $Al_{68.75}Cu_{18.75}Fe_{12.5}$ and for $Al_{50}Cu_{37.5}Fe_{12.5}$. The dominant s character feature has reduced width and a shifted center with respect to the $Al_{50}Cu_{37.5}Fe_{12.5}$ result. For $Al_{68.75}Cu_{18.75}Fe_{12.5}$, the dominant s-character feature has its maximum 7.4 eV below E_F, in the center of the feature, and extends 2 eV in each direction from the center. There are two smaller, prominent peaks of s character: Both have similar intensity. The position of these two peaks is 2 eV from E_F and at E_F, indicating interaction with Fe d states for both features. For the p-character Al DOS, the maximum has position indicative of mixing with the Cu d states. Between E_F and 6 eV below E_F, the Al p DOS is relatively unstructured and the existing structures have similar intensity. This is a noticeable difference from the $Al_{50}Cu_{37.5}Fe_{12.5}$ case where the interaction with Fe d states leads to a peaked feature about 1.6 eV from E_F. We attribute the above differences between the $Al_{50}Cu_{37.5}Fe_{12.5}$ and $Al_{68.75}Cu_{18.75}Fe_{12.5}$ spectra to the fact that for the former, the second-nearest-neighbor of Fe is Cu; whereas for the latter, Fe has Al as a second-nearest neighbor.

IV. DISCUSSION

Let us recall that the experimental curves reflect the product $|M|^2\mathcal{N}(E)^*\mathcal{L}(E)$ where M is the matrix element of the x-ray transition probability, $\mathcal{N}(E)$ is the partial DOS, and $\mathcal{L}(E)$ a Lorentzian function whose FWHM intensity is the energy width of the inner level involved in the x-ray transition. We have already mentioned that the transition probabilities are nearly constant in the investigated energy range. So, to compare the theoretical results with the experimental ones, we have simulated theoretical x-ray spectra as follows: we have broadened each partial calculated DOS by a convenient $\mathcal{L}(E)$ function and, to account for the instrumental functions of our apparatus, we have smoothed the result by suitable Gaussian (G) functions. The widths of the $\mathcal{L}(E)$ and G functions are given in Table VI taken from Ref. 35.

For the Cu $3d$ and Fe $3d$ distributions in all the alloys, the agreement is good between experiment and the calculated x-ray curves. As an example, this is shown in Fig. 13 for Fe $3d$ states distribution in Al_7Cu_2Fe.

Figure 14 displays two sets of curves for Al_2Cu. Almost all the features existing in the calculated curves are seen on the experimental ones; however, some discrepancies are observed. For Al $3p$ distribution, the calculated and the experimental edges are not superposed (upper curves); the most striking discrepancy arises from the fact that the calculated Al $3p$ and Al $3d$ distributions exhibit

TABLE VI. Full width at half maximum for the Lorentzian and Gaussian curves used to calculate theoretical x-ray transitions.

	$\mathcal{L}$	G
Al $3s,d$	0.1	0.3
Al $3p$	0.5	0.2
Al p	0.5	0.5
Fe $3d$	0.4	0.3
Fe d,s	0.4	0.4
Cu $3d$	0.6	0.5
Cu d,s	0.6	0.4

features not observed in the experimental ones. As an example, to the two maxima labeled A and B of the calculated curves correspond minima, labeled, respectively, A' and B' in the experimental ones. This suggests that the calculation overestimates the p-d and d-d interactions between Al and Cu, especially in the center of the occupied band.

The same kind of discrepancies are observed for the OB of Al_7Cu_2Fe; but, in that case, the edges of both calculated and experimental curves are rather well superposed. However, as seen in Fig. 15 for the Al $3p$ states, the calculation does not explain the structure A that is seen in the experimental curve. At this energy, Fe $3d$ states are present in the OB and in this energy range the calculation may underestimate the interaction between Al and Fe states. The presence of the extra peak at the position of the step at about 4 eV from E_F seen on the experimental curve affects the intensities of all the features of the calculated partial DOS's.

Figures 16(a) and 16(b) show a comparison between the experimental and calculated x-ray spectra, respectively, for Cu and Fe d,s conduction states in Al_7Cu_2Fe. For Cu, the experimental edge is between those corresponding to the calculated d and s spectra. The shape of the experimental curve is rather similar to that of the calculated d spectrum, but decreases abruptly beyond about 4 eV from E_F. Consequently, the Cu conduction states are d-s hybridized but more d-like. For Fe, the feature labeled A is superposed to the edge of the Al p and Fe p curves not shown here (see Fig. 4). Feature B coincides with the maximum of the calculated curve related to d states. Calculated s states are located beyond 3 eV from E_F; thus, the Fe conduction states are hybridized d-p in interaction with Al p states near E_F, then almost d-like and d-s-like.

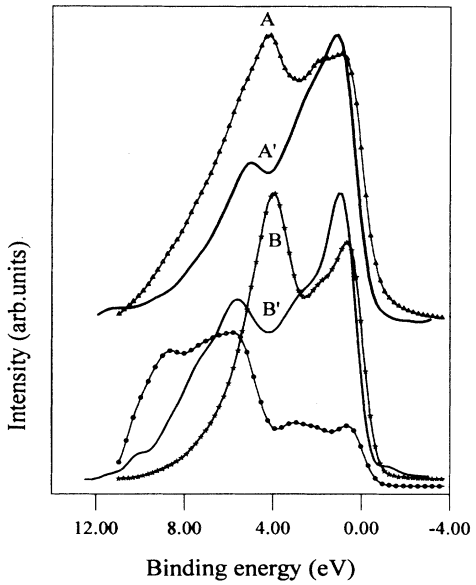

FIG. 14. Partial Al valence-band distributions of Al_2Cu: * lower curves: solid line is the experimental Al $3s,d$ distribution, line with full circles is Al $3s$ calculated x-ray curve, line with stars is Al $3d$ calculated x-ray curve, * upper curves: solid line is experimental Al $3p$ distribution, line with triangles is Al $3p$ calculated x-ray curve.

For $Al_{50}Cu_{37.5}Fe_{12.5}$, the Al calculated, broadened spectra are examined closely and compared to the experimental spectra of $Al_{55}Cu_{33}Fe_{12}$ and $Al_{46}Cu_{36}Fe_{18}$ (shown in Fig. 3).[36] For the Al $K\beta$ spectra (Al $3p$ states), the position of the peaks are in good agreement, but the relative intensity of the peaks is reversed with respect to the ex-

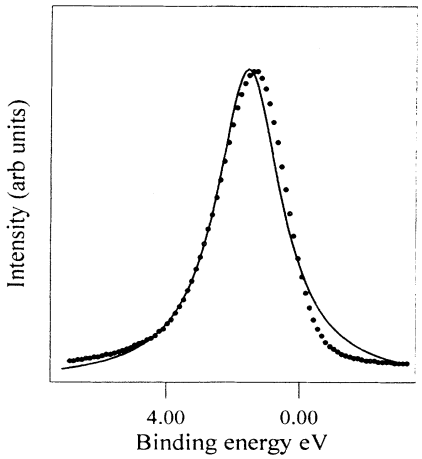

FIG. 13. Fe $3d$ curves in Al_7Cu_2Fe: experimental is the thick solid line and calculated is the line with full circles.

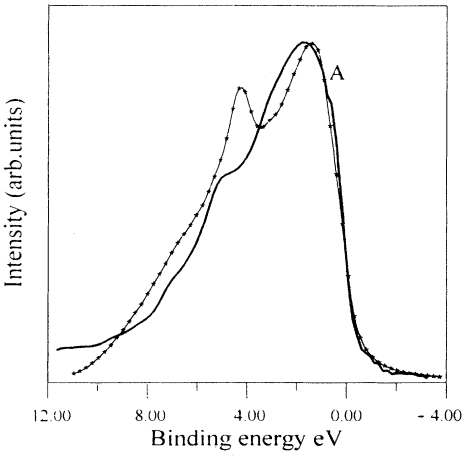

FIG. 15. Al $3p$ x-ray curves in Al_7Cu_2Fe: experimental (solid line) and calculated for all the Al sites (line with stars).

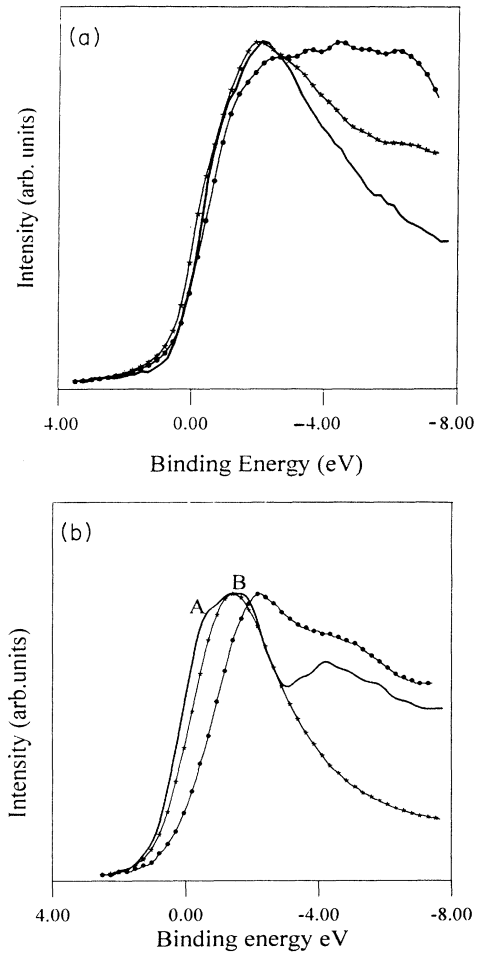

FIG. 16. (a) x-ray curves in Al_7Cu_2Fe: experimental Cu *s,d* (solid line) and calculated (line with stars, Cu *d*: line with full circles, Cu *s*). (b) x-ray curves in Al_7Cu_2Fe: experimental Fe *s,d* (solid line) and calculated (line with stars, Fe *d*: line with full circles, Fe *s*).

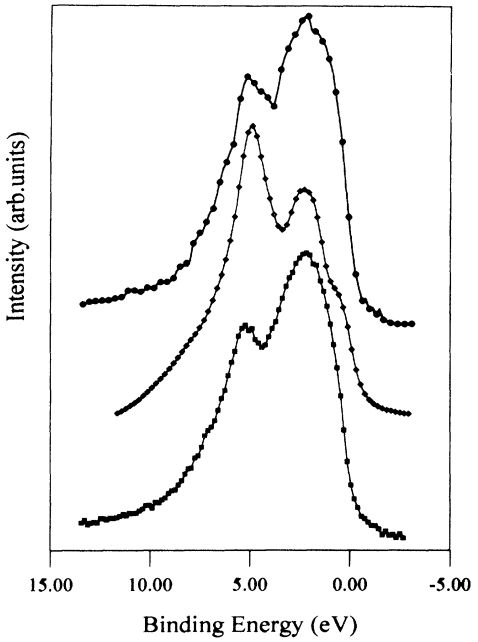

FIG. 17. Comparison between calculated Al $K\beta$ spectrum for $Al_{50}Cu_{37.5}Fe_{12.5}$ (line with diamonds) and experimental Al $K\beta$ spectra for $Al_{46}Cu_{36}Fe_{18}$ (upper curve, line with circles) and $Al_{55}Cu_{33}Fe_{12}$ (lower curve, line with squares).

perimental curves (Fig. 17). For the *L* spectra, a similar situation exists between theoretical and experimental curves. In this case, however, there is some question about oxide contribution to the experimental results in an energy range centered about 5 eV from E_F. When the experimental spectra are compared with the calculated spectra for $Al_{68.75}Cu_{18.75}Fe_{12.5}$, the *L* spectrum shows improved agreement with respect to the relative intensity of the peaks, but shows a shift in the position of the peak nearer to E_F and of the minimum between the two peaks of the curves [Fig. 18(a)]. The *K* spectrum calculated for $Al_{68.75}Cu_{18.75}Fe_{12.5}$ is significantly different from the experimental spectrum and the spectrum calculated for $Al_{50}Cu_{37.5}Fe_{12.5}$. For $Al_{68.75}Cu_{18.75}Fe_{12.5}$, the calculated *K* spectrum shows only one distinct structured peak [Fig. 18(b)]. These discrepancies emphasize the sensitivity of Al to its neighbors.

Let us now compare the Al 3*p* distributions in crystalline Al_7Cu_2Fe and in quasicrystalline $Al_{63}Cu_{25}Fe_{12}$. Figure 19 displays the experimental curve for the quasicrystal and calculated Al 3*p* curves for each Al site in Al_7Cu_2Fe. The experimental curve exhibits a rounded shape beyond the edge. Accounting for this bending of the experimental curve and for the width of the principal peak near its maximum intensity, it seems that the calculated curve for site Al (2) is the one that could be compared to the experiment.[37] However, it is necessary to make the assumption that in the quasicrystal, the strength of the interaction between the Al *p-d* hybridized states and the Fe 3*d* states near E_F is very different than in the crystalline alloy. Indeed, when going from Al_7Cu_2Fe to the quasicrystalline phase, we observe an important depletion of the Al states that are present near the Fermi level: the effect of which is to shift the Al 3*p* occupied band edge towards the center of the OB, giving rise to a notable pseudogap at E_F. So we suggest that in the Al-Cu-Fe quasicrystals, the Al-Fe interaction is noticeably stronger than in Al_7Cu_2Fe and that Al is located in sites analogous to site Al (2) in the ω phase; in these sites, Al has Fe but no Cu atoms as close neighbors.

V. CONCLUSION

The experimental techniques used in this study allowed us to measure partial densities of states associated to *s* and *d* or *p* orbitals; thus, they are particularly well adapted to the study of systems where hybridization and interaction between *p* and *d* bands is important. Indeed, for Al_7Cu_2Fe, we find that interaction between *p-d* states of Al and *d* states of the transition elements is important especially near the Fermi energy. Such an interaction seems to be even more pronounced in the case of

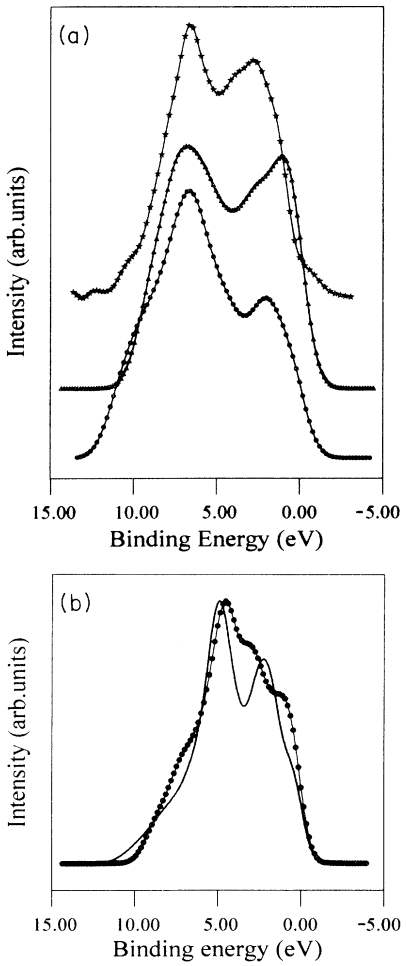

FIG. 18. (a) Calculated Al $L_{2,3}$ spectra in $Al_{68.75}Cu_{18.75}Fe_{12.5}$ (line with triangles) and in $Al_{50}Cu_{37.5}Fe_{12.5}$ (line with circles); expermental Al $L_{2,3}$ spectrum in $Al_{46}Cu_{36}Fe_{18}$ (line with stars). (b) Calculated Al $K\beta$ spectra in cubic $Al_{50}Cu_{37.5}Fe_{12.5}$ (solid line) and cubic $Al_{68.75}Cu_{18.75}Fe_{12.5}$ (line with circles).

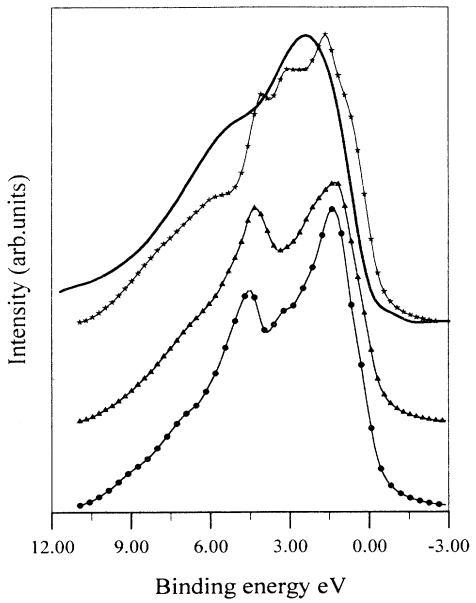

FIG. 19. Comparison between experimental Al 3*p* curve for quasicrystalline icosahedral $Al_{63}Cu_{25}Fe_{12}$ alloy (thick solid line) and calculated Al 3*p* x-ray curves for crystalline Al_7Cu_2Fe (line with circles, site Al [1]: line with triangles, site Al [3]: line with stars, site Al [2]).

the quasicrystalline $Al_{63}Cu_{25}Fe_{12}$ alloys. We note also that crystalline $Al_{68.75}Cu_{18.75}Fe_{12.5}$ and $Al_{50}Cu_{37.5}Fe_{12.5}$ phases display somewhat different electronic structures. This is seen particularly for the whole Fe *d* DOS as well as in the DOS near E_F. Roughly speaking, the structures corresponding to these alloys are obtained replacing Fe atoms by Cu atoms in a cubic Al-Fe cell. The DOS calculations emphasize that this replacing of Fe by Cu leads to important changes in the electronic distributions. In other words, this shows that Al atoms are very sensitive to their close neighbors, i.e., the pseudopotentials of Fe and Cu atoms should play a significant role in the electronic structure and consequently the electronic properties of all these systems. We have observed a very good agreement between theory and experiment for Fe and Cu spectra. Discrepancies are mainly in the Al spectra, which appear to be very sensitive on the neighbor atoms. Therefore, we attribute the discrepancies between theory and experiment to the fact that most of our calculations have assumed stoichiometries and atom positions that do not reflect precisely enough those of the measured samples.

ACKNOWLEDGMENTS

Dr. Yvonne Calvayrac, Dr. Mireille Harmelin, and Dr. Claire Berger are warmly acknowledged for kindly providing us with crystalline and quasicrystalline well-characterized samples. We are indebted to Professor F. Cyrot-Lackmann, Professor T. Fujiwara, and Professor A. Switendick for stimulating discussions. One of us (Z.D.) acknowledges financial support from TEMPUS Contract No. HUS-017-91 and BGF Contract No. 92/108.

[1]J. Friedel and F. Dénoyer, C. R. Acad. Sci. **T305**, 171 (1987).
[2]M. Mori, S. Matsuo, T. Ishimasa, T. Matsuura, K. Kamiya, H. Inokuchi, and T. Matsukawa, J. Phys. Condens. Matter **3**, 767 (1991).
[3]E. Belin and A. Traverse, J. Phys. Condens. Matter **3**, 2157 (1991).
[4]E. Belin, Z. Dankhazi, A. Sadoc, Y. Calvayrac, T. Klein, and J. M. Dubois, J. Phys. Condens. Matter **4**, 4459 (1992).
[5]E. Belin and Z. Dankhazi, J. Non-Cryst. Solids **153&154**, 298 (1993).
[6]A. Sadoc, E. Belin, Z. Dankhazi, and A. M. Flank, J. Non-Cryst. Solids **153&154**, 338 (1993).

[7]Z. M. Stadnik and G. Stroink, Phys. Rev. B **47**, 100 (1993).
[8]S. Matsuo, H. Nakano, T. Ishimasa, and Y. Fukano, J. Phys. Condens. Matter **1**, 6893 (1989).
[9]Z. Dankhazi, G. Trambly de Laissardière, D. Nguyen Manh, E. Belin, and D. Mayou, J. Phys. Condens. Matter **5**, 3339 (1993).
[10]G. Trambly de Laissardière, D. Mayou, and D. Nguyen Manh, Europhys. Lett. **21**, 25 (1993).
[11]T. Fujiwara, Phys. Rev. B **40**, 942 (1989).
[12]T. Fujiwara, Solid State Commun. **117&118**, 844 (1990).
[13]T. Fujiwara and T. Yokokawa, Phys. Rev. Lett. **66**, 333 (1991).
[14]D. A. Papaconstantopoulos, *Handbook of the Band Structure of Elemental Solids* (Plenum, New York, 1986), p. 205.
[15]P. Léonard, J. Phys. F **8**, 467 (1978).
[16]J. C. Fuggle, E. Källne, L. M.Watson, and D. J. Fabian, Phys. Rev. B **16**, 750 (1977).
[17]A. E. Dunsworth, J. P. Jan, and H. L. Skriver, J. Phys. F **9**, 1077 (1979).
[18]O. K. Andersen, Phys. Rev. B **12**, 3060 (1975).
[19]O. K. Andersen, O. Jepsen, and D.Glotzet, in *Highlights of Condensed Matter Theory,* edited by F. Bassani, F. Fumi, and M. P. Tosi (North-Holland, New York, 1985), p. 59; R. W. G. Wyckoff, Cryst. Struct. **1**, 363 (1948), Eq. (59).
[20]W. B. Pearson, *Handbook of Lattice and Structures of Metals and Alloys* (Pergamon, London, 1967), p. 99.
[21]J. M. Friauf, J. Am. Chem. Soc. **49**, 3107 (1927).
[22]G. Lehman and M. Taut, Phys. Status Solidi B **54**, 469 (1972).
[23]B. M. Bown and P. J. Brown, Acta Crystallogr. **9**, 911 (1956).
[24]*Pearson's Handbook of Crystallographic Data for Intermetallic Phases,* edited by P. Villars and L. D. Calvert (American Society for Metals, Metals Park, OH, 1985), p. 211, Eq. (85).
[25]O. K. Andersen, O. Jepsen, and M. Sob, *Electronic Band Structure and Its Application,* edited by M. Yussoff, Springer Lecture Notes in Physics Vol. 283 (Springer-Verlag, Berlin, 1987), p. 1.
[26]D. Nguyen Manh, G. Trambly de Laissardière, J. P. Julien, D. Mayou, and F. Cyrot-Lackmann, Solid State Commun. **82**, 329 (1992).
[27]N. E. Christensen, Phys. Rev. B **32**, 207 (1985).
[28]U. von Barth and L. Hedin, J. Phys. C **5**, 1629 (1972).
[29]J. C. Slater, Phys. Rev. **51**, 846 (1937); L. F. Matheiss, J. H. Wood, and A. Switendick, *Methods in Computational Physics 8,* edited by A. Adler, S. Fernbach, and R. Rotenberg (Academic, New York, 1968), p. 63.
[30]L. Hedin and B. I. Lundqvist, J. Phys. C **4**, 2064 (1971).
[31]G. P. Srivastava, J. Phys. A **17**, L317 (1984).
[32]L. L. Boyer, Phys. Rev. **18**, 2824 (1979).
[33]D. A. Goodings and R. Harris, J. Phys. C **2**, 1808 (1969).
[34]D. Mayou, in *Lectures on Quasicrystals,* edited by F. Hippert and D. Gratias (Les Editions de Physique, Les Ulis, 1994), p. 417.
[35]M. O. Krause and J. H. Oliver, J. Phys. Chem. Ref. Data **8**, 329 (1979).
[36]M. A. Keegan and D. A. Papaconstantopoulos, in *Nanophase Materials: Synthesis, Properties, Applications,* edited by G. C. Hadjipanayis and R. W. Siegel (Kluwer, Dordrecht, 1994), p. 323.
[37]E. Belin, Z. Dankhazi, and A. Sadoc, Mater. Sci. Eng. A **181-182**, 717 (1994).